Δελτίο της Ελληνικής Γεωλογικής Εταιρίας, 2010
Πρακτικά 12ου Διεθνούς Συνεδρίου
Πάτρα, Μάιος 2010

Bulletin of the Geological Society of Greece, 2010
Proceedings of the 12th International Congress
Patras, May, 2010

SEGMENTATION AND INTERACTION OF NORMAL FAULTS IN CENTRAL GREECE

Kokkalas S.

University of Patras, Department of Geology, Laboratory of Structural Geology, 26500 Patras, Greece, skokalas@upatras.gr

Abstract

The aim of this study is to improve our understanding on the mechanical interaction and linkage process between normal fault segments. Faults grow by the process of radial propagation and the linkage of segments, as strain increases, evolving to large fault systems. For this purpose we conducted a combined field and photogeological study on two major segmented fault zones in Central Greece, the Atalanti and Arkitsa fault zones. This approach includes effects of fault size and spatial distribution, scaling laws and footwall-hanginwall topography. Throw distribution and the geometry of the segmented fault arrays were analyzed in order to investigate the complexity of fault zones, the fault linkage process and the geometric characteristics of the relay zones formed between individual segments. The correlation of fault throw with fault length (D-L) and the ratios of overlap-separation (OL-S), separation-fault segment length (S-L) and relay displacement vs. separation (Dr-S) were examined in order to give an insight for fault segment interaction and linkage .

Key words: *fault segmentation, fault geometry, relay zones, Arkitsa-Atalanti fault zones, Evoikos Gulf.*

1. Introduction

Displacements on normal faults are rarely accommodated on a single well-defined slip surface, but are partitioned between interacting fault segments (Walsh and Watterson, 1991; Peacock and Sanderson, 1991; Cartwright et al., 1995; Willemse, 1997). Fault segmentation occurs across a wide range of length scales (Stewart and Hancock, 1991; Trudgill and Cartwright, 1994; Walsh et al., 2003) and faults can be observed as isolated or discontinuing sub-parallel stepping segments with overlapping or underlapping configuration. The transfer of displacement from one fault segment to another, dipping in the same direction, most often occurs through relay structures (Larsen, 1988). These are zones of high fault-parallel shear strain that provide soft linkage (Walsh and Watterson, 1991) between two interacting fault segments (Fig. 1). Breaching occurs when the fault segments are replaced by a single, through-going fault surface. Interaction and linkage between fracture segments have been studied in regimes of thrust and strike-slip faulting (Aydin and Schultz, 1990; Segall and Pollard, 1980; An 1997) and more recently between segments of extension fractures and normal faults in continental areas (Childs et al. 1995; Acocella et al., 2000; Soliva and Benedicto; 2004). All past works aimed to improve comprehension of mechanical interaction and linkage processes between faults, including the effects on scaling laws and growth models of faults as well as in fault size and spatial distribution. The linkage of individual fault segments into faults is critical for understanding the fault array's behaviour. Thus, the degree of fault segment linkage can modify earthquake sequences and

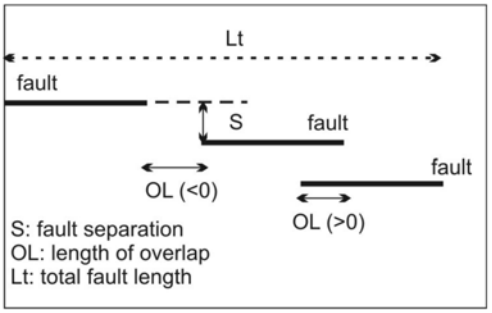

Fig. 1: Simplified illustration showing the main structural features of an interacting fault array and the relay zone terminology used here. S is the width of relay zone or the fault segments separation/overstep, while OL is the length of overlap between them. When OL<0 we have an underlapping configuration while when OL>0 we have an overlapping configuration.

magnitudes because a fault array can possibly act as a single fault (Gupta and Scholtz, 2000; Cowie and Roberts, 2001), indicating in this way its importance in understanding natural seismic hazards.

The purpose of this paper is to shed some light and explore the way in which fault growth by fault linkage influences the development of a fault population that initially has a power-law distribution of lengths.

2. Geological setting

In central Greece, much of the extensional strain is localised into a number of WNW-ESE trending grabens, which are mostly characterised by complex geometries in map view (Fig.1B), and a high degree of segmentation along strike (Doutsos & Poulimenos, 1992; Ganas et al., 1998; Kokkalas et al., 2006). Most of the major range bounding normal faults are thought to have been active in the Pleistocene, but the relative time of their activity is not well constrained.

The study area comprises a series of mainly north-dipping normal fault segments that define the southern boundary of the North Gulf of Evia in central Greece. This graben is one of several seismically active zones of N-S to NE-SW regional extension, with rates on the order of 1-2 mm/yr (Clarke et al. 1998), generally inferred to accommodate mechanical interaction of the North Anatolian–Aegean Trough strike-slip fault system and the Hellenic subduction zone (Doutsos and Kokkalas, 2001; Kokkalas et l. 2006). Basin bounding faults of these grabens are often well exposed where they juxtapose Mesozoic carbonates in their footwalls with Neogene sediments in their hanging walls. Slip on the Arkitsa fault zone, although poorly constrained, is likely to significantly exceed the 300–400 m topographic relief of the associated footwall block, with minimum throw possibly around 500-600 m (Kokkalas et al. 2007). Thus, a slip rate of 0.2-0.3 mm/yr can be calculated for Arkitsa fault zone, taking into account that faults of Evia rift zone started their activity in the last 2-3 My (Ganas et al. 1998). Slip rates for the adjacent Atalanti fault show similar values on the order of 0.27-0.4 mm/yr (Ganas et al. 1998).

The Arkitsa fault zone, together with Ag. Konstantinos fault (AKF) and Kamena Vourla fault (KVF), form a WNW-ESE left stepping, north-dipping fault margin that link with the southern margin of the Almyros-Sperchios graben (Fig.1). The Arkitsa fault zone, which has a length of ~10 km, separates Late Triassic – Jurassic platform carbonates in the footwall from Lower Pliocene to Quaternary sediments in the hangingwall. The geomorphological expression of Arkitsa region, the back-tilted terraces on the hanginwall block of Arkitsa fault, as well as the fresh ~1m band of unweathered limestone at the contact between the scree and fault plane before the quarrying, suggest Holocene seismic activity along this fault. Additionally, the coastline in the region shows evidence of Holocene uplift and subsidence that is controlled by the motion and location of the faults (Roberts & Jackson, 1991; Stiros et al. 1992).

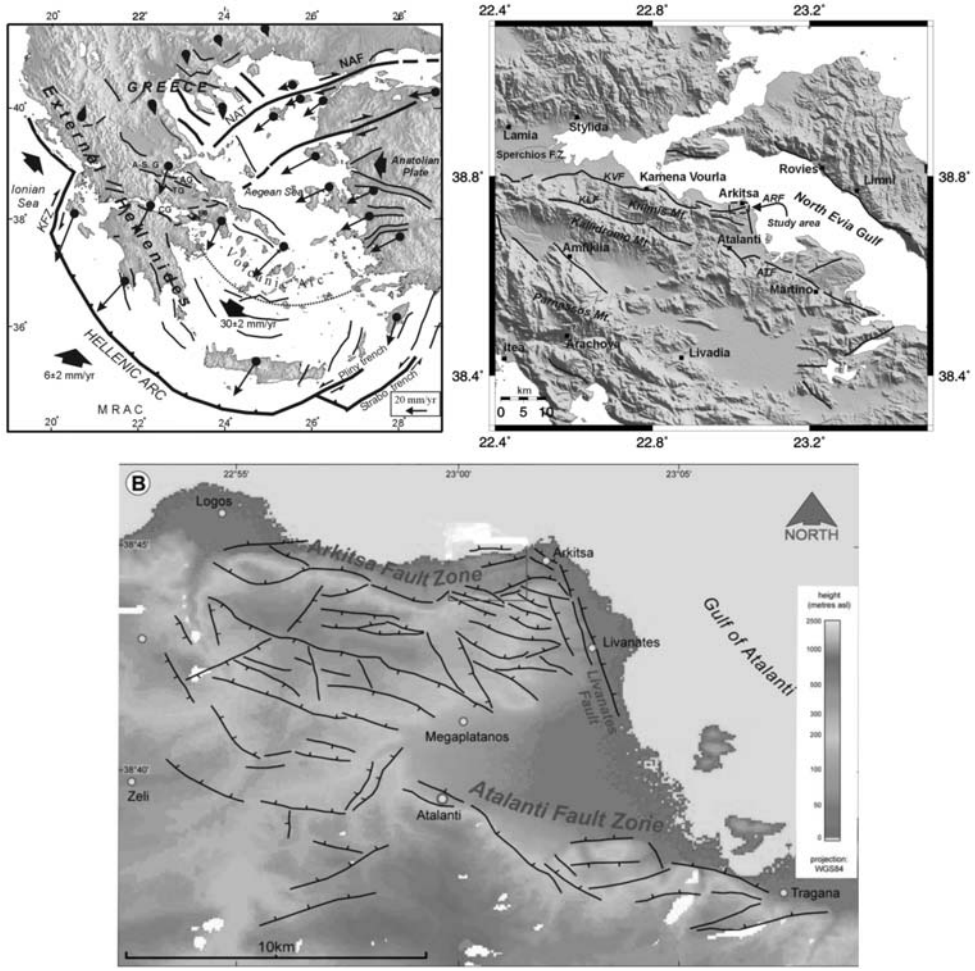

Fig. 2: (up left): Simplified map showing the main structural features along the Hellenic Peninsula, as well as the main active structures. The mean GPS horizontal velocities in the Aegean plate are shown with respect to a Eurasia fixed reference frame. CG: Corinth graben, TG: Tithorea graben, AG: Atalanti graben, A-S.G: Almyros-Sperchios graben, MB: Megara basin. NAT: North Aegean Trough, NAF: North Anatolia Fault, KFZ: Kephalonia transform fault, MRAC: Mediterranean Ridge Accretionary Complex. Map modified from Kokkalas et al. (2006); (up right): Map of central Greece close to the North Evia Gulf showing the main fault traces and the study area (arrow pointing to dashed rectangle). ATF: Atalanti fault, ARF: Arkitsa Fault; KLF: Kallidromo fault, KVF: Kamena Vourla fault. (B. down) Tectonic map of the broader study area. The Arkitsa and Atalanti fault zones are shown on map.

3. Fault zone characteristics

The knowledge of fault dimensions has become a powerful tool on many applications such as the estimation of strain in a region (Marrett and Almendinger 1992, Koukouvelas et al. 1999) and proposing models for fault growth (Walsh et al. 2002; Kim and Sanderson, 2005).

For this purpose we analyzed almost 70 fault traces (Fig. 2B) between Atalanti and Arkitsa fault zones. Beyond the published data, the mapping of faults was derived analysis of aerial photographs

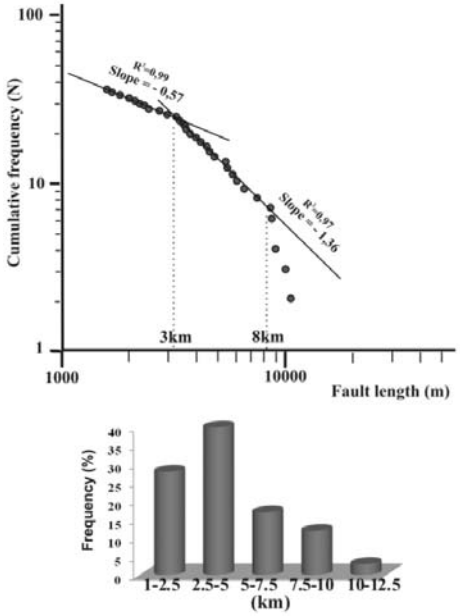

Fig. 3: Log-Log plot of the cumulative frequency with fault length and histogram of frequency with fault length for the faults of the broader study area.

(scale 1:17000) and DTM analysis in areas of poor data collection. Most faults and especially the two studies fault zones of Arkitsa and Atalanti are segmented along strike. Thus, fault segment showing tip areas and maximum throw near to fault center can be regarded as prominent fault segments. From their topographic profiles they appear to have a half spoon footwall shape and display abrupt changes in strike and trend of adjacent segments.

For the histogram of frequency versus fault length, from the studied area, we used data from combined photogeological and field work (Fig. 3). Almost 70% of the fault population is represented by faults with lengths <5 km. Gaps on lengths below 1.5 km can be related to the scale of observation.

3.1 Fault size

Fault size (i.e. displacement and length) has been proposed to be characterized by a power-law distribution (e.g., Marrett and Allmendinger, 1992; Poulimenos, 2000; Walsh et al., 2003). Generally, the population distribution can be expressed as

$$N = c\, U^{-D}, \tag{1}$$

where N is number of faults with a displacement greater than U, c is a constant, and D is the power-law exponent on the cumulative frequency plot. For this equation, an increasing value of D implies a greater number of small faults relative to large faults.

The published values for D of individual datasets ranges from 0.67 to 2.07 (e.g., Cladouhos and Marrett, 1996; Xu et al., 2006). Changes of D-value are due to both measurement and natural process (e.g., Yielding et al., 1996).

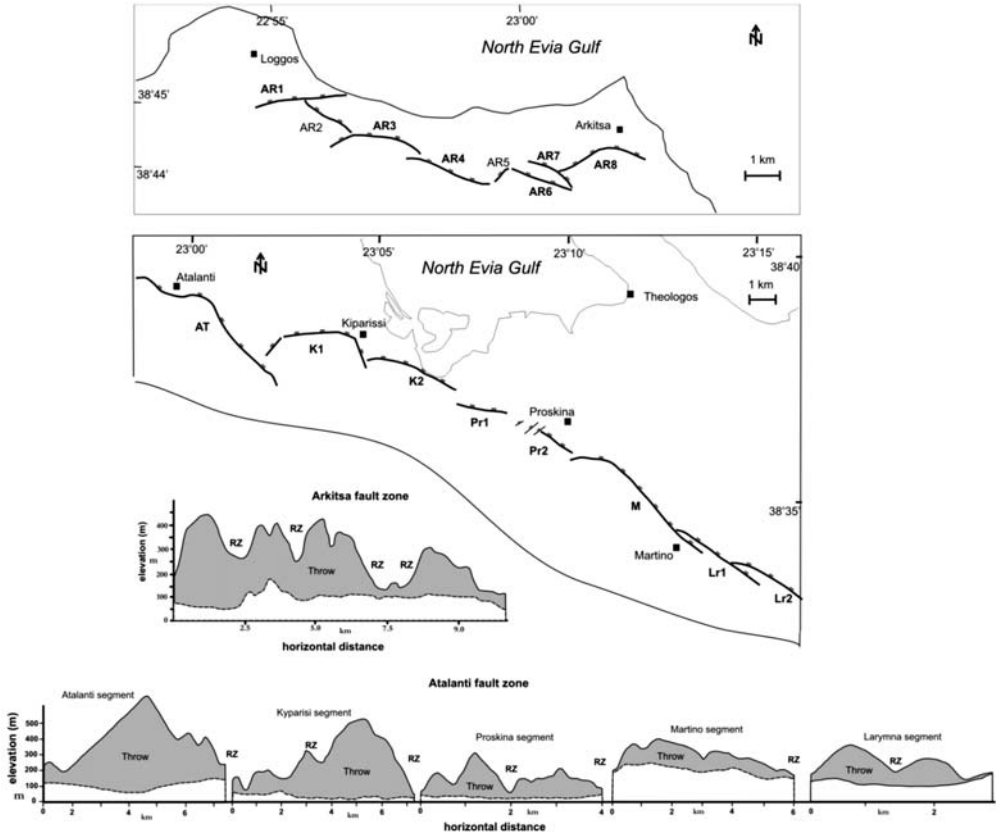

Fig. 4: Simplified maps of the Arkitsa and Atalanti fault zones showing the fault zone segmentation. Below, footwall & hanginwall elevation profiles, derived from DEM's, showing the variation of throw on each fault segment along strikes, are displayed.

For example, if the connectivity of distinct fault trace exposures cannot be observed, the estimated power-law exponents will be higher because the lengths of the faults appear to be smaller. On the other hand, it has been recognized that fault linkage causes the power-law exponent (D) to decrease in progressive deformation (Cladouhos and Marrett, 1996; Wojtal, 1996). This effect is documented by the physical experiments of Mansfield and Cartwright (2001). The systematic variations of the power-law exponent have been explained by strain localization onto progressively fewer and larger faults (Walsh et al., 2003), and have been predicted from physical experiments and numerical models (Cowie et al., 1995; Cladouhos and Marrett, 1996).

Fault length–cumulative frequency data are displayed in log–log graphs in order to identify sampling artifacts that stem from sampling area dimensions and sampling resolution. For the faults in the broader study area a logarithmic plot of the cumulative frequency of faults (N) vs. fault trace length (L) is displayed in Fig.3 Break in the graph indicates that the distribution is multi-fractal with two straight segments fitting the data (bi-fractal), with D-value of 0.57 for fault lengths <3 km and 1.36 for lengths between 3 and 8 km. Frequency distributions comprise the inherent shortcoming of truncation of small-scale features and finite range effect of large-scale features, that were excluded from

our linear relationships (Yielding et al., 1992; Pickering et al., 1995). D value (1.36), for the normal faults with lengths ranging from 3 to 8 km, testifies an increase in the importance of smaller structures contributing relatively more in strain accommodation of the area. Steps on the data-plot presented in Fig.3 subdivide the curve into two distinct sectors and indicate that within fault population there are abrupt increases and decreases in the number of faults at particular length scales (3 km and 8 km). The two sectors of the cumulative distribution may reflect different stages of evolution between fault arrays. Thus, they can be considered to account for fault linkage that replaces two smaller faults within the population with one larger fault (Mansfield and Cartwrigth, 2001).

3.2 Fault throw profiles

The fault zones of Atalanti and Arkitsa, affecting the southern coast of North Evia Gulf were mapped in detail from aerial photography and field observations. Footwall and hanginwall elevation profiles were derived from DEM (SRTM data, 90 m) showing also the variation of fault throw on each fault segment. Depending on scale of observation, these two fault zones are considered to be more or less segmented. For example in the Atalanti fault zone, Pavlides et al. (2004) suggested that this zone comprises five main segments that are also shown in the elevation profile of Fig. 4.

Footwall topography and local highs and lows along strike reveal that some of the main segments are also segmented into smaller segments (Fig. 4). For example, in Atalanti fault zone with the exception of western Atalanti segment, which appears to be a single segment with high amount of displacement, all other fault segments seem to be composed by two smaller segments having various stages of linkage. So, in this study we suggest that Atalanti zone comprises eight segments with a total length of 31.3 km. In a similar way, Arkitsa fault zone is also segmented along strike into five main segments (Ar1-Ar3-Ar4-Ar6-Ar8) with ENE and WNW orientation, while another three segments with NW (Ar2-Ar7) and NE (Ar5) orientations are aligned along the relay zones between the main segments (Fig. 4). More detail studies (i.e. terrestrial laser scanning) on the well-known segment of Arkitsa fault (Kokkalas et al. 2007) showed that this segment is also segmented into another three fault panels, with lengths on the order of 100-300 m and with high degree of curvature (Jones et al. 2009).

From the footwall-hanginwall topographic profiles, a noteworthy characteristic is that fault throw isn't always symmetric and close to fault segment centre as expected in isolated faults but it displays asymmetry towards the tip zone of the neighbouring fault segment, usually towards the west (Fig. 4).

3.3 D/L diagrams

The vertical throw on fault segments is used in this study as a proxy of the displacement, as is suggested also by Anders and Schlische (1994) and Dawers and Anders (1995).

The relationship between maximum displacement and fault length can be described as:

$$d_{max} = cL^n \quad (2)$$

(Cowie and Scholz, 1992; Scholz et al., 1993; Dawers et al., 1993). Attempts to determine the parameter n concluded in n = 2 (Watterson 1986; Walsh and Watterson, 1988), n = 1.5 (Marrett and Allmendinger, 1991; Gillespie et al., 1992) and n = 1 (Gudmundsson, 1992; Dawers et al., 1993). Cowie and Roberts (2001) suggest that the way in which a fault grows is fundamentally denoted by the ratio of maximum displacement to length. During the initial stage of coalescence a linked fault's length is the sum of the lengths of the smaller fault segments, while the maximum displacement remains the greatest value of the individual fault segment. In order for the scaling relationships to be

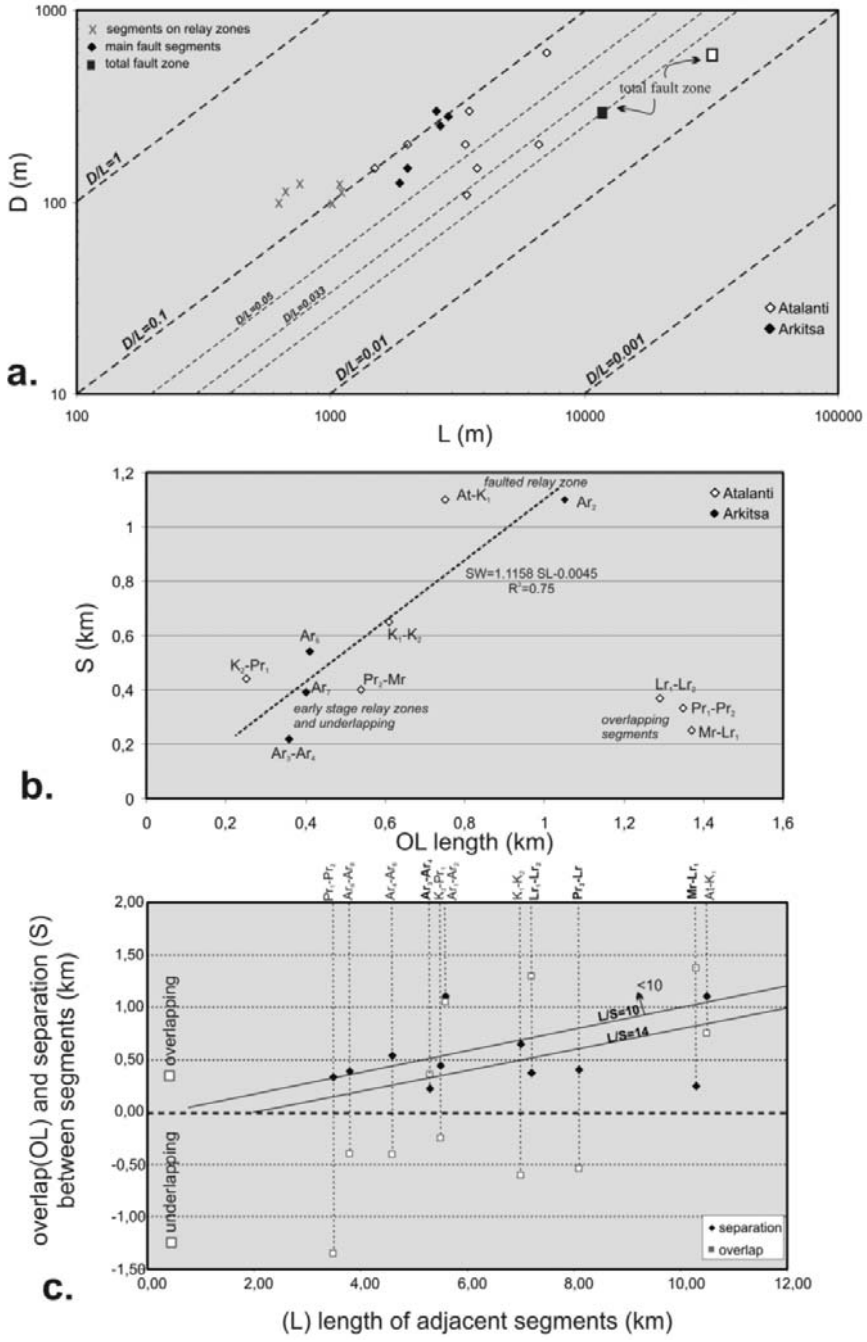

Fig. 5: a) Displacement-length diagram for all fault segments, relay zones as well as for the total length of fault zone b) Separation/overstep versus overlap/underlap length for the studied fault zones and c) Diagram of overlap and separation versus total length of the segments from both sides of the relay zone.

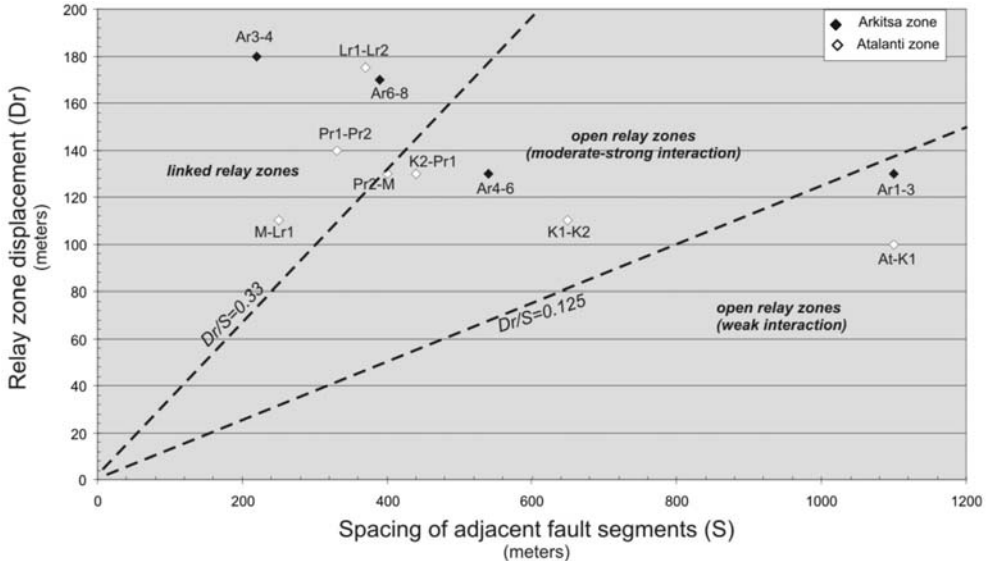

Fig. 6: Graph of relay displacement (Dr) vs. separation (S) of he different types of studied relay zones from Arkitsa and Atalanti. Areas are bounded by specific values of Dr/S.

generally applicable, maximum displacement must be accommodated in large fault structures as a whole because treating fault segments as individual faults generally generates larger dmax/L ratios (Peacock and Sanderson, 1991; Vermilye and Scholz, 1995).

Use of a logarithmic plot of maximum throw vs. fault trace length, for 18 well constrained fault segments (Fig. 5a) shows that the d/L data are bounded between a group of straight lines (Fig. 5a) representing dmax/L ratios between 0.02 and 0.3. Although restrictions such as host lithology and earthquake history must not be disregarded, in general fault populations seem to have similar systematic increase of displacement with length increase. Fault populations suggest that especially for faults <4 km long, throw varies more than one order of magnitude. Since a fault can develop through successive slip events on an individual segment or a group of them, the dmax/L ratio increase depends on the distribution of these events and the rate of fault propagation. Taking into account that segmentation is largely observed within the study area, thereafter, the dmax/L ratio is expected to attain high values in more matured linked faults. The reason why the dmax/L ratios are lower in some cases (i.e. Atalanti fault zone) maybe due to footwall erosion that reduces the displacement. Thus fault populations have d/L values lying beneath the growth line, with growth paths reflecting their own specific history of linkage. It appears that faults lengthen faster at a time, and after evolve their length and throw variably.

Diagram of Fig. 5a shows a general trend towards increasing D with L, but with scatter of about one order of magnitude in D with constant length. The D:L data define a linear band bounded by a pair of parallel straight lines with D/L ratios equal to 0,03 and 0.1. The data from Arkitsa are clustered above a line with a ratio of 0.05 while for Atalanti data are more uniformly distributed to the broad band. Note that the data points for the entire fault length of Arkitsa and Atalanti fall below the data of major fault segments. This can be interpreted as the result of displacement transfer across relay structures, which show higher D/L ratios, (Fig. 5a), which is also associated with steep displacement gradients at segment tips.

D/L systematic displays a change in fault geometry and evolution, where larger strain is represented by incremental increase in displacement than incremental increase in length.

4. Relay zones' geometry

Fracture interaction during propagation of adjacent fracture tips can include several stages. In a first stage underlapping tips of main fractures began to curve outwards from their earlier straight pathway while in a later stage they can develop a hook-shape geometry. In a more progressive stage segments can breach into a single continuous fracture. Relay ramps occur between fault segments that overstep in map view. Characteristic variability in displacement-distance profiles for fault segments and linked faults accompanies the interaction and linkage processes. Displacement transfer by relay ramps is accompanied by steep displacement gradients along fault segments at oversteps. Relay ramps often contribute to a minimum in total fault displacement at a linkage point.

Separation (S) and overlap (OL), the geometric parameters that used to represent relay zone scaling and fault segment interaction are easy to obtain on map views (Aydin and Schultz, 1990). An important measure of the architecture of relay zones is the aspect ratio A = OL/S, where OL is the length of the overlap (or underlap) zone and S is the separation/overstep between fractures (Fig. 5b). The relay zones in the study area display aspect ratios from 0.57 to 5.48 (mean value is 1.99 and s.d. is 1.72). The great majority of values cluster around value 1, while high values (are represented by highly overlapping relay zones (Lr1-Lr2, M-Lr1), as well as by initially collinear fractures (S almost 0; Pr1-Pr2) that show en echelon geometry in the relay zone (see Table 1 and Fig. 4). In general, higher OL/S ratio is consistent with a more evolved stage in fault overlap and linkage. Fault interaction and linkage occur earlier during fault overlap for small values of separation than large ones. Relationship between OL and S from a broad range of scales showed mean values of 4.9 (from normal faults; Acocella et al. 2000) and around 4.7 (for strike slip faults; Aydin and Schultz, 1990).

For a given overstep there is a critical minimum length for the fractures to interact and overlap; below this value interaction and overlap is inhibited. Acocella et al. (2000) suggests that this minimum length appears to be almost 14 times the overstep (S) between fractures, while sandbox models yield similar minimum values (about 10 times the overstep S) in strike-slip settings (An 1997) for linkage to occur. In Fig. 5c, relay zones with higher potential to interact and link are the M-Lr1, Pr2-M and Lr1-Lr2 zones between Martino, Larymna and west Proskina fault segments for the Atalanti zone, while for Arkitsa zone only the Ar3-Ar4 relay zone displays the highest L/S ratio. Great part of the rest of relay zones display values around 10.

We also used a relay displacement-separation diagram in order to define a segment criterion considering that the amount of displacement at relay ramp and fault separation/overstep control the fault's ability to link during overlap (Fig. 6). Relay displacement (Dr), which is the sum of displacement of each fault segment at tip zone, and fault segment separation (S) are measured on the relay ramp on a line normal to the ramp strike and at the centre of the overlap (or underlap) length. The results are presented on Fig. 6 for both the Arkitsa and Atalanti zones. Open relays exhibit low values of ratio Dr/S less than 0.125 and represent relay zones with weak interaction. Open relays with moderate to strong interaction show values between 0.125 and 0.3. Finally, linked relay zones with the highest potential for initiation of linkage and breaching display values above 0.33. Linked relays represent zones in which fault segments link when relay displacement increases during overlap or tip to tip linkage. Results for the linked relay zones fit well with the L/S values mentioned above. None of the studied relay zones display characteristics of fully breaching since they need to display values of Dr/S from a minimum of 0.8 to 1< (see also Soliva and Benedicto, 2004).

Based on the above and according to the segment length of the mapped faults and the potential for interaction and linkage, we used the empirical relationships of Wells and Coppersmith (1994), Ambraseys and Jackson (1998) and Pavlides and Caputo (2004) in order to make a first estimation for the seismic potential magnitude for each fault zone. In table 2, the seismic magnitude is given for each pair of segments with higher potential to interact and link, as well for the whole zone, according to the above mentioned empirical relationships. The Atalanti and Arkitsa Fault zones give a magnitude of 6.82-6.83 and 6.28-6.45 respectively, as is estimated for the worst scenario for total fault length activation, while for all other cases a magnitude between 5.8 and 6.5 is estimated.

5. Conclusions-Results

In cumulative frequency against fault length plots, fault linkage produces shallower slopes near the linked length scales. This effect directly results in fluctuating curves when fault linkage at different length scales occurs. For fault linkage, the size of the linked faults is a fundamental factor that influences the development of a fault population that initially has a power law distribution of lengths. The smallest linked faults result in an increase in the power-law exponent, as seems to be the case for the whole study area, whereas the largest linked faults result in a reduction of the power-law exponent.

A growing fault array characterized by accruing displacement but no significant lateral propagation is "saturated" sensu Wu and Pollard (1995) and in a later stage the increase of d/L suggests the array "matures" sensu Walsh et al. (2002). Multi-fractal properties are observed on well-developed fault networks and are referred to the existence of distinct fault subsets, or reveal fracture mechanism. Our bi-fractal distribution suggests that the two populations are saturated and mature (Fig. 3). Based on the cumulative distribution (Fig. 3), we recognize two characteristic lengths at approximately 3 km and 8 km.

The d/L ratio changes significantly during the fault evolution stages or shows irregularities and scatter due to interaction and linkage between faults, as individual faults grow at different stages of development. The displacement on a particular fault segment or relay zone becomes proportionally larger as interaction increases because fault propagation is inhibited (see also Peacock and Sanderson 1996). Data from Arkitsa show higher values of D/L than Atalanti area and this indicate a more mature stage in the fault array evolution.

Relationships between overlap/underlap, separation, relay displacement and length of the adjacent segments of Atalanti and Arkitsa faults can be used to discriminate relay zones with weak or stronger interaction. The western segments of Atalanti zone (Proskina-Martino and Larymna segments) as well as the central segments of Arkitsa fault (Ar3-Ar4) indicate a stronger interaction and more progressive stage for fault linkage. Additionaly, these segments display the highest value of fault segment length vs. separation (L/S) as well as relay displacement to separation ratio (Dr/S).

In any case of fault rupture scenario an earthquake of magnitude around 6-6.5 is possible in case of reactivation of any pair of these segments, although the study area appears to be in low risk since it displays low strain (Hollenstein et al. 2008) and long recurrence intervals for past strong earthquakes based on paleoseismological studies (Pantosti et al.2004.; Pavlides et al. 2004).

6. Acknowledgments

The author would like to thank the two anonymous reviewers for their suggestions and M. Zambos for discussion on diagram results.

Appendix 1

Table 1. Fault segments and relay zone geometry characteristics.

Fault segment	Length (m)	Throw (m)	Relay displ. (m)	Overlap (m)	Separation (m)	Ratio OL/S
		Atalanti Fault zone				
At	7100	600				
			100	750	1100	0.69
K1	3460	200				
			110	-600	650	0.93
K2	3500	300				
			130	-250	440	0.57
Pr1	1970	200				
			140	-1350	330	4.09
Pr2	1520	150				
			130	-540	400	1.35
Mr	6580	200				
			110	1370	250	5.48
Lr1	3800	150				
			175	1290	370	3.49
Lr2	3400	110				
		Arkitsa Fault zone				
Ar1	2900	280				
Ar2	1700	130	130	1050	1100	0.96
Ar3	2700	250				
			180	360	220	1.64
Ar4	2600	300				
Ar5	660	130	130	-410	540	0.76
Ar6	1970	150				
Ar7	1530	170	170	-400	390	1.03
Ar8	1880	125				

Table 2. Potential magnitudes for fault segment reactivation. Abbreviation of fault segments names same as in Figure 4.

Fault	Length (km)	Wells & Coppersmith (1994)[*1]	Ambraseys & Jackson (1998)[*2]	Pavlides & Caputo (2004)[*3]
Ar_3-Ar_4	5.3	5.81	5.95	6.13
At	7.1	5.98	6.10	6.24
K_1-K_2	7	5.97	6.09	6.24
Ar_3-Ar_4-Ar_6-Ar_8	9.15	6.12	6.22	6.35
Pr_1-Pr_2-M-Lr_1-Lr_2	17.0	6.48	6.53	6.5
Arkitsa F.Z. total	12	6.28	6.36	6.45
Atalanti F.Z. total	31.3	6.83	6.83	6.82

[*1]Wells & Coppersmith (1994): Ms=1.32logL+4.86, L: length of fault
[*2]Ambraseys & Jackson (1998): Ms= 5.13+1.14logL, L : length of fault
[*3]Pavlides & Caputo (2004): Ms=0.9log (SRL)+5.48, SRL=surface rupture length

7. References

Acocella, V., Gudmundsson, A., Funiciello, R., 2000. Interaction and linkage of extensional fractures: examples from the rift zone of Iceland. *J. Struct. Geol.,* 22, 1233–1246.

Ambraseys, N.N. and Jackson, J.A., 1998. Faulting associated with historical and recent earthquakes in the Eastern Mediterranean region. *Geophys. J. Int.*, 133, 390-406.

An, L., 1997. Maximum link distance between strike-slip faults: observations and constraints. *PAGEOPH.,* 150, 19–36.

Anders, M.H., Schlische, R.W., 1994. Overlapping faults, intrabasin highs, and the growth of Normal faults. *J. Geol.* 102, 165–180.

Aydin, A., Schultz, A., 1990. Effect of mechanical interaction on the development of strike-slip faults within echelon patterns. *J. Struct. Geol.,* 12, 123–129.

Cartwright, J.A., Trudgill, B.D., Mansfield, C.S., 1995. Fault growth by segment linkage: an explanation for scatter in maximum displacement and trace length data from the Canyonlands Grabens of SE Utah. *J. Struct. Geol.,* 17, 1319–1326.

Childs, C., Watterson, J., Walsh, J.J., 1995. Fault overlap zones within developing normal fault systems. *J. Geol. Soc., London*, vol. 152, 535-549.

Cladouhos, T.T., Marrett, R., 1996. Are fault growth and linkage models consistent with power-law distributions of fault lengths? *J. Struct. Geol.,* 18, 281-293.

Clarke, P.J., and 13 others, 1998. Crustal strain in central Greece from repeated GPS measurements in the interval 1989–1997. *Geophys. J. Int.*, 135, p. 195–214, doi: 10.1046/j.1365-246X.1998.00633.x.

Cowie, P.A., Scholz, C.H., 1992. Growth of faults by accumulation of seismic slip. *J. Geophys. Res.,* 10, 11085-11095.

Cowie, P.A., Roberts, G.P., 2001. Constraining slip rates and spacings for active normal faults. *J. Struct. Geol.,* 23, 1901–1915.

Cowie, P.A., Sornette, D., Vanneste, C., 1995. Multifractal scaling properties of growing fault population. *Geophys. J. Int.* 122, 457–469.

Dawers, N.H., Anders, M.H., Scholz, C.H., 1993. Growth of normal faults: displacement–length scaling. *Geology* 21, 1107–1110.

Dawers, N.H., Anders, M.H., 1995. Displacement–length scaling and fault linkage. *J. Struct. Geol.,* 17, 607–614.

Doutsos, T., Poulimenos, G., 1992. Geometry and kinematics of active faults and their seismotectonic significance in the western Corinth-Patras rift (Greece). *J. Struct. Geol.,* 14, 689-699.

Doutsos, T., Kokkalas S. 2001. Stress and deformation in the Aegean region. *J. Struct. Geol.,* 23, 455-472.

Ganas, A., Roberts, G., Memou, P., 1998. Segment boundaries, the 1894 ruptures and strain patterns along the Atalanti fault, central Greece. *J. Geodyn*., 26, 461-486.

Gillespie, P.A., Walsh, J.J., Watterson, J., 1992. Limitations of dimension and displacement data from single faults and the consequences for data analysis and interpretation. *J. Struct. Geol*. 14, 1157–1172.

Gudmundsson, A., 1992. Formation and growth of normal faults at the divergent plate boundary in Iceland. *Terra Nova* 4, 464–471.

Gupta, A., Scholz, C., 2000. A model of normal fault interaction based on observations and theory. *J. Struct. Geol.,* 22, 865–879.

Hollenstein, C., Muller, M.D., Geiger, A., and Kahle, H.-G.,2008. Crustal motion and deformation in Greece from a decade of GPS measurements, 1993–2003. *Tectonophysics*, 449, 17–40, doi: 10.1016/j.tecto .2007.12.006

Jones, R.R., Kokkalas, S., McCaffrey, K.J.W., 2009. Quantitative analysis and visualization of nonplanar fault surfaces using terrestrial laser scanning (LIDAR)-The Arkitsa fault, central Greece, as a case study. *Geosphere*, 5, 465-482; doi: 10.1130/GES00216.1

Kim, Y.-S., Sanderson, D.J., 2005. The relationship between displacement and length of faults: a review. *Earth Sci. Rev*. 68, 317–334.

Kokkalas, S., Jones, R.R., McCaffrey, K.J.W., Clegg, P., 2007. Quantitative fault analysis at Arkitsa, Central Greece, using terrestrial laser-scanning ("LiDAR"). *Bull. Geol. Soc. Greece,* XXXVII, 1959-1972.

Kokkalas, S., Xypolias, P., Koukouvelas, I., and Doutsos, T. 2006. Postcollisional contractional and extensional deformation in the Aegean region, *in* Dilek, Y., and Pavlides, S., eds., Post-collisional tectonics and magmatism in the Mediterranean region and Asia: *Geol. Soc. Am. Special Paper 409*, 97–123, doi: 10.1130/2006.2409(06)

Koukouvelas, I.K., Asimakopoulos, M., Doutsos, T., 1999. Fractal characteristics of active normal faults: an example of the eastern Gulf of Corinth, Greece. *Tectonophysics*, 308, 263–274.

Larsen, P.H., 1988. Relay structures in a Lower Permian basement involved extension system. East Greenland. *J. Struct. Geol.,* 10, 3-8.

Mansfield, C., Cartwrigth, J., 2001. Fault growth by linkage: observations and implications from analogue models. *J. Struct. Geol*. 23, 745–763.

Marrett, R.A., Allmedinger, R.W., 1991. Estimates of strain due to brittle faulting: sampling of fault populations, Kinematic analysis of fault-slip data. *J. Struct. Geol.,* 13, 735-738.

Marrett, R., Allmendinger, R.W., 1992. Amount of extension on 'small' faults: an example from the Viking graben. *Geology,* 20, 47–50.

Pantosti, D., De Martini, P.M., Papanastassiou, D., Lemeille, F., Palyvos, N., and Stavrakakis, G., 2004. Paleoseismological Trenching across the Atalanti Fault (Central Greece): Evidence for the Ancestors of the 1894 Earthquake during the Middle Age and Roman Times. *Bull. Seism. Soc. America*, 94, 2, 531-549.

Pavlides, S.B. and Caputo, R., 2004. Magnitude versus fault's surface parameters: quantitative relationships from the Aegean Region. *Tectonophysics*, 380, 3-4, 159-188.

Pavlides S.B., Valkaniotis S., Ganas A., Keramydas D. and Sboras S. 2004 The Atalanti active fault: reevaluation using new heological data. Bull. Geol. Soc. Greece. XXXVI, *Proceedings of the 10th International Congress*, Thessaloniki, 1560-1567.

Peacock, D.C.P., Sanderson, D.J., 1991. Displacements, segment linkage and relay ramps in normal fault zones. *J. Struct. Geol.,* 13, 721-733.

Peacock, D.C.P., Sanderson, D.J., 1996. Effects of propagation rate on displacement variations along faults. *J. Struct. Geol.,* 18, 311-320.

Pickering, G., Bull, J.M., Sanderson, D.J., 1995. Sampling power law distributions. *Tectonophysics* 248, 1-20.

Poulimenos, G., 2000. Scaling properties of normal fault populations in the western Corinth Graben, Greece: implications for fault growth in large strain settings. *J. Struct. Geol.* 22, 307–322.

Roberts, S., and Jackson, J., 1991. Active normal faults in central Greece: An overview, *in* Holdsworth, R.E., and Turner, J.P., compilers, Extensional tectonics: Faulting and related processes: Key Issues in Earth Sciences, Volume 2: London. *Geol. Soc. London*, 151–168.

Scholz, C.H., Dawers, N.H., Yu, J.Z., Anders, M.H., Cowie, P.A., 1993. Fault growth and fault scaling laws: preliminary results. *J.Geophys. Res.*, 98, 21951–21961.

Segall, P., Pollard, D.D., 1980. Mechanics of discontinuous faults. *J.Geophys. Res.*, 85, No B8, 4337-4350.

Soliva, R., Benedicto, A., 2004. A linkage criterion for segmented normal fa*ults. J. Struct. Geol.*, 26, 2251-2267.

Stiros, S.C., Arnold, M., Pirazzoli, P.A., Laborel, J., Laborel, F., and Papageorgiou, S., 1992. Historical coseismic uplift on Euboea Island, Greece. *Earth Plan. Sci. Lett.*, 108, 109–117, doi: 10.1016/0012-821X(92)90063-2

Trudgill, B., Cartwright, J., 1994. Relay-ramp forms and normal ault linkages, Canyonlands national Park, Utah. *Geol. Soc. Am. Bull.*, 106, 1143-1157.

Vermilye, J.M., Scholz, C.H., 1995. Relation between vein length and aperture. *J. Struct. Geol.* 17, 423–434

Walsh, J.J., Watterson, J., 1991. Geometric and kinematic coherence and scale effects in normal fault systems. *Geol. Soc., London, Special Publications*, 56, 193-203.

Walsh, J.J., Nicol, A., Childs, C., 2002. An alternative model for the growth of faults. *J. Struct. Geol.* 24, 1669–1675.

Walsh, J.J., Bailey, W.R., Childs, C., Nicol, A., Bonson, C.G., 2003. Formation of segmented normal faults: a 3-D perspective. *J. Struct. Geol.*, 25, 1251-1262.

Watterson, J., 1986. Fault dimensions, displacements and growth. *Pure Appl.Geophys.* 124, 365–373.

Wells, D.L. and Coppersmith, K.J., 1994. New empirical relationships among magnitude, rupture length, rupture width, rupture area and surface displacement. *Bull. Seism. Soc. America*, 84, 974-1002.

Willemse, E.J.M., 1997. Segmented normal faults: Correspondence between three-dimensional mechanical models and field data. *J. Geophys. Res.*, 102 (B1), 675-692.

Wojtal, S.F., 1996. Changes in fault displacement populations correlated to linkage between faults. *J. Struct. Geol.* 18, 265–279.

Wu, H., Pollard, D.D., 1995. An experimental study of the relationship between joint spacing and layer thickness. *J. Struct. Geol.,* 17, 887-905.

Xu, S.-S., Nieto-Samaniego, A.F., Alaniz-Alvarez, S.A., Velasquillo-Martinez, L.G., 2006. Effect of sampling and linkage on fault length and length–displacement relationship. *Int. J. Earth Sci.* 95, 841–853.

Yielding, G., Walsh, J.J., Watterson, J., 1992. The prediction of small-scale faulting in reservoirs. *First Break* 10, 449-460.